

# Multi-unit soft sensing permits few-shot learning

Bjarne Grimstad<sup>1, 2, a</sup>, Kristian Løvland<sup>1, 2, b</sup> and Lars S. Imsland<sup>1, c</sup>

<sup>1</sup>Norwegian University of Science and Technology, Trondheim,  
Norway

<sup>2</sup>Solution Seeker AS, Oslo, Norway

<sup>a</sup>[bjarne.grimstad@ntnu.no](mailto:bjarne.grimstad@ntnu.no) (Corresponding author)

<sup>b</sup>[kristian.lovland@ntnu.no](mailto:kristian.lovland@ntnu.no)

<sup>c</sup>[lars.imsland@ntnu.no](mailto:lars.imsland@ntnu.no)

September 28, 2023

## Abstract

Recent literature has explored various ways to improve soft sensors using learning algorithms with transferability. Broadly put, the performance of a soft sensor may be strengthened when it is learned by solving multiple tasks. The usefulness of transferability depends on how strongly related the devised learning tasks are. A particularly relevant case for transferability, is when a soft sensor is to be developed for a process of which there are many realizations, e.g. system or device with many implementations from which data is available. Then, each realization presents a soft sensor learning task, and it is reasonable to expect that the different tasks are strongly related. Applying transferability in this setting leads to what we call multi-unit soft sensing, where a soft sensor models a process by learning from data from all of its realizations.

This paper explores the learning abilities of a multi-unit soft sensor, which is formulated as a hierarchical model and implemented using a deep neural network. In particular, we investigate how well the soft sensor generalizes as the number of units increase. Using a large industrial dataset, we demonstrate that, when the soft sensor is learned from a sufficient number of tasks, it permits few-shot learning on data from new units. Surprisingly, regarding the difficulty of the task, few-shot learning on 1-3 data points often leads to a high performance on new units.

---

\* © 2023 IEEE. Personal use of this material is permitted. Permission from IEEE must be obtained for all other uses, in any current or future media, including reprinting/republishing this material for advertising or promotional purposes, creating new collective works, for resale or redistribution to servers or lists, or reuse of any copyrighted component of this work in other works.

*Keywords:* soft sensor, hierarchical model, neural network, multi-task learning, few-shot learning

## 1 Introduction

In many processes there are variables of interest that are hard to measure. An example would be a key performance indicator that cannot be measured directly, or whose measurement requires an expensive or disruptive experiment. The purpose of developing *soft sensors* for such processes is to make cheap and timely inferences about the variables of interest, based on other variables that are more accessible.

In essence, a soft sensor is a mathematical model that operates on available process measurements ( $x$ ) to infer a variable of interest ( $y$ ). Two important assumptions in the development of a soft sensor are i) that the process measurements are informative of  $y$ , and ii) that the process measurements arrive with a higher frequency than measurements of  $y$ . In application, the soft sensor is used to indirectly monitor  $y$  at times when only  $x$  is measured. Furthermore, when  $y$  is a key performance indicator, the process can be optimized based on the inferred values.

The literature on soft sensing and its applications is extensive and presents several decades of progress; see [1, 2, 3]. *On-line prediction*, as described above, is the most common application of soft sensors and the focus of this paper. Soft sensors are also developed for other applications, including process monitoring, fault detection, and sensor reconstruction, which will not be considered here.

The last decade of the literature can be characterized by the stream of works that have adopted recent advancements in data science, particularly within deep learning, to soft sensing [4, 5]. Many of these works target the process industry, whose expansion and increasing complexity demands new, cost-efficient soft sensor technologies [6, 7].

**Data-driven soft sensors** Arguably, the most common form of a soft sensor is  $E[y | x; \theta] = F(x; \theta)$ , where the conditional expected value of  $y$  is modeled by a function  $F$  with arguments  $x$  and parameters  $\theta$ . A soft sensor can be classified as being either *model-based* or *data-driven*, based on the specification of  $F$  [2]. In a model-based soft sensor,  $F$  is derived from first-principles. For example,  $F$  may be a mechanistic model whose parameters represent physical properties of the process being modeled. In a data-driven soft sensor,  $F$  is a generic function to be fitted to data. For example,  $F$  may be a linear regression model or neural network with parameters  $\theta$ . Regardless of the soft sensor type, the model should be calibrated to available measurement pairs  $\{(x, y)\}$  before being used for prediction. Commonly used methods include least-squares or maximum likelihood estimation (MLE). If a prior density is available for  $\theta$ , maximum a posteriori (MAP) estimation or Bayesian inference can be used to calibrate the model [8].

Two advantages of model-based soft sensors are: first, that they can be applied to any realization of the process, provided  $F$  is a valid process model; second, that they are data-efficient since the number of parameters is small. For first-principles models, the parameters are interpretable, which can allow meaningful priors to be imposed, further improving the data efficiency. One disadvantage of model-based soft sensors is that they can be expensive or difficult to develop and maintain, especially when the modeled variable  $y$  is explained by complex phenomena. Furthermore, for a real process, any model will be an approximation, and if the model is too simple it may not have the capacity to fit the observed data, leading to local calibration and poor generalization.

The disadvantages of model-based soft sensors have motivated much of the development of data-driven soft sensors. The attraction to data-driven soft sensing comes from its promise to simplify and reduce the cost of modeling by learning the model from historical data using statistical inference or machine learning techniques. The main challenge in data-driven soft sensing is arguably to learn a model from information-poor data. The paucity of information may be due to a low data volume, measurement frequency, variety, or quality [2]. The challenge is closely tied to the motivation for implementing a soft sensor, i.e., to infer a key variable that is measured infrequently. Put differently, a soft sensor is most valuable in information-poor environments, where one would expect data-driven methods to perform poorly. To achieve a good predictive performance in such environments, it is imperative to be *data efficient*. Model-based soft sensors achieve this by having few parameters and strong priors. Data-driven soft sensors, which may have more model parameters than observations to learn from, rely on using generic regularization techniques and weak priors.

Another disadvantage with many data-driven soft sensors is that their model must be learned from scratch for each realization of a process, even when the two realization are known to be similar. As such, they are not able to take full advantage of the data when it consists of observations from multiple process realizations.

**Soft sensor transferability** A recent theme in the soft sensing literature is transferability, or transfer learning [9, 5, 10]. Simply put, transfer learning entails taking knowledge acquired by solving a source task and utilizing it to improve generalization on a target task [11]. Here, a task would be to develop a soft sensor. The knowledge, captured by a model, is then transferred from one soft sensor (source) to the next (target). The model learned on the source task may act as a stronger prior than an generic or uninformative prior on the target task, and in this way improve the data efficiency.

The *multi-task learning* (MTL) paradigm generalizes the unidirectional transfer (described above) to multidirectional transfer between two or more tasks [12]. With MTL, multiple soft sensors are learned simultaneously and knowledge transfer is enabled through hard or soft parameter-sharing [10, 13].

Transferability, either via transfer learning or MTL, can be used in different ways to improve soft sensors. Here, we discuss recent attempts to employ trans-

ferability along four “dimensions”: across data fidelity (e.g. from synthetic to real data), across domains (e.g. operating conditions), across target variables (e.g. quality indicators), and across processes (e.g. similar but physically different processes).

In [14], a soft sensor was developed by first training on synthetic data generated by a first-principles simulator, and then fine-tuning the model on a limited amount of real process data. In this case, transfer learning provided a mechanism for combining real and synthetic data to improve the model. A draw-back with the approach is that it requires a first-principles simulator.

It is often the case that the operating practices, operating conditions, or dynamics of industrial processes induce a data shift, e.g. a covariate shift, meaning that the source-domain data is differently distributed than the target-domain data. Transfer learning across different operating conditions is referred to as *cross-phase transfer learning* in [9]. As demonstrated in [15], cross-phase transfer learning can enhance the soft sensor performance on the target domain. Operating conditions can also change due to sensor faults. Fault-tolerant soft sensors can then be developed using techniques from domain adaptation, a subcategory of transfer learning [16].

In many processes there are multiple target variables, e.g. different key performance indicators or quality indicators, for which soft sensors are developed. When these target variables are related, it may be beneficial to transfer learn across the soft sensors [17, 18, 19, 13]. As an example, consider a manufacturing plant which does not work as intended, leading to an overall poor product quality and correlation among quality indicators.

Finally, knowledge can be transferred between soft sensors for similar, but physically different processes. This setting is referred to as *cross-entity transfer learning* in [9]. Many soft sensors are developed for designed processes; consider a soft sensor developed for a specific pump unit, which may be of a model produced in large numbers. With data from multiple units (i.e. process realizations), soft sensor performance may be improved by multi-task learning across units. One example is given in [20], where a data-driven virtual flow meter is learned from data from many oil wells. Below, we elaborate on this application of MTL, where a task represents a soft sensor for a unit. We refer to this as *multi-unit soft sensing*.<sup>1</sup>

**Multi-unit soft sensing** Consider  $M$  units with soft sensor models  $F_1(x; \theta_1)$ , ...,  $F_M(x; \theta_M)$ , where  $\theta_i$  are the parameters of model  $i = 1, \dots, M$ . When multi-unit soft sensing is implemented as MTL with hard parameter-sharing, a subset of the parameters are shared by all unit models, while some are unit-specific. Let  $\theta$  denote shared parameters and let  $\{c_1, \dots, c_M\}$  be unit-specific parameters. Then we can write  $F_i = F(x; \theta, c_i)$  for unit  $i$ , which makes it

---

<sup>1</sup>We use the term *unit* to refer to a realization of a process being modeled by a soft sensor. More concretely, units may refer to a set of objects, e.g. pumps, valves, or solar panels, or a set of complex systems, such as distillation columns, oil wells, or robots. In other works, a unit may be referred to as an entity, subject, object, or realization for which we have one or more observations.

clear that we can represent all the soft sensors by one parameterized function,  $F$ . This conjoined model can improve data efficiency by learning the shared parameters,  $\theta$ , using data from all units. A common way to implement MTL with deep neural networks, is to share all of the hidden layers, and to have one output layer per task [12]. This results in a high number of shared parameters, and task-specific parameters that are lower-dimensional.

The framing of (data-driven) multi-unit soft sensing allows us to draw an interesting parallel to model-based soft sensing. Imagine a case where  $F$  is learned from a large dataset. If the dataset contains observations from a sufficiently large number of units, one could expect that  $\theta$  converges to a stationary point (or at least to a neighborhood of a stationary point). Suppose that we, after having learned  $F$  from this dataset, are presented with a new unit. Then, we may consider the model  $G(x; c) = F(x; \theta, c)$ , where  $\theta$  is fixed, assuming that it has converged. Thus, we may utilize the data of the new unit to calibrate only the low-dimensional unit-parameters  $c$ . In machine learning terminology, this would be an example of *few-shot learning*, where a model can solve a task after being calibrated to a few (often less than ten) data points [21, 22]. The learned model  $G$  (or  $F$  with  $\theta$  fixed) can then be thought to represent the modeled process. The non-fixed  $c$  parameters must then capture the specificities of the units; similarly to how the parameters of a first-principles model represent the physical properties of units. However, the  $c$  parameters will remain abstract, unlike the interpretable parameters of a first-principles model.

**Contributions** Our work is centered on multi-unit soft sensing and its learning capabilities. Specifically, we present two findings from an empirical study on a large-scale industrial case.

- The average soft sensor performance (across units) increases with the number of units. The convergence rate matches a theoretical estimate, and can be used to indicate when a good base model is found.
- A base model trained on many units, enables few-shot learning on other units. In our case, calibration of unit-specific parameters to only one or two observations leads to a low prediction error for new units.

We believe that our findings are relevant for industrial applications of multi-unit soft sensing. First, the scaling properties indicate that soft sensors with good generalizability can be developed from multi-unit datasets. Second, the demonstrated few-shot learning capability enables the application of data-driven soft sensors in data-scarce settings. For units with few observations, many have considered model-based or hybrid soft sensors to be the only suitable solution; see e.g. [23, 14]. This opens up for running and calibrating (or fine-tuning) purely data-driven soft sensors on edge computing hardware, where computational resources are limited [24]. This may be particularly interesting to manufacturing or service companies that want to bundle soft sensors with their hardware offers.

As discussed above, others have formulated multi-unit soft sensing as an application of MTL; e.g. [20]. Subsequently, we frame it as a hierarchical modeling problem, where model parameters enter at different levels to capture variations among units and observations. We propose a probabilistic model where nonlinearities are represented by a deep neural network, and a learning method based on stochastic gradient descent. This framework, which uses fairly standard components, cannot be considered novel. A similar framework has been applied in other works, e.g. for meta learning [22].

**Structure of paper** The paper proceeds by giving a mathematical problem formulation in Section 2. The multi-unit soft sensor model is then described in Section 3, followed by the derivation of the learning method in Section 4. An empirical study based on a large-scale industrial dataset is presented in Section 5. Finally, concluding remarks are given in Section 6. Some implementation details and additional results are gathered in the appendix.

**Notation** A parametric function  $f$  with inputs  $(x, y)$  and parameters  $(a, b)$  is denoted by  $f(x, y; a, b)$ , where the input and parameter arguments are separated by a semicolon.

Sets of variables are compactly represented by bold symbols, e.g.  $\mathbf{x} = \{x_i\}_{i=1}^N$ , where  $x_i \in \mathbb{R}^D$  for some positive integers  $D$  and  $N$ . For double-indexed variables we write  $\mathbf{x} = \{x_{ij}\}_{ij}$  when the index sets of  $i$  and  $j$  are implicit. When the indices are irrelevant to the discussion, we may write  $x$  instead of  $x_{ij}$ .

For some positive integer  $K$ , we denote the  $K$ -vector of zeros by  $0_K$  and the  $K \times K$  identity matrix by  $I_K$ . For a  $K$ -vector  $\sigma = (\sigma_1, \dots, \sigma_K)$ ,  $\log(\sigma)$  denotes the element-wise natural logarithm,  $\exp(\sigma)$  the element-wise natural exponential, and  $\text{diag}(\sigma^2)$  denotes the diagonal  $(K \times K)$ -matrix with diagonal elements  $(\sigma_1^2, \dots, \sigma_K^2)$ .

The normal distribution is denoted by  $\mathcal{N}(\mu, \Sigma)$ , where  $\mu$  is a mean vector and  $\Sigma$  is a covariance matrix. If  $X$  is normally distributed random variable, we denote a sample by  $x \sim \mathcal{N}(x | \mu, \Sigma)$ . Generally, we use the letter  $p$  to denote a probability distribution,  $p(x)$ , or a conditional probability distribution,  $p(y | x)$ . We sometimes use the letter  $q$  for probability distributions that are approximative.

## 2 Problem statement

Consider a set of  $M > 1$  distinct, but related *units* indexed by  $i \in \{1, \dots, M\}$ . The units are assumed to be related so that it is reasonable to expect, a priori to seeing data, that transfer learning between units is beneficial. For each unit  $i$ , we have at our disposal a set of  $N_i$  observations  $\mathcal{D}_i = \{(x_{ij}, y_{ij})\}_{j=1}^{N_i}$ , where  $x_{ij} \in \mathbb{R}^D$  denotes explanatory variables and  $y_{ij} \in \mathbb{R}$  are target variables. We assume that the variables represent similar measurements or quantities across units. We also assume that each dataset  $\mathcal{D}_i$  consists of independent and identically

distributed (iid.) observations drawn from a probability distribution  $p_i(x, y) = p_i(y|x)p_i(x)$  over  $\mathbb{R}^D \times \mathbb{R}$ .

Our goal is to efficiently learn the behavior of the units, as captured by the conditional densities  $p_1(y|x), \dots, p_M(y|x)$ , from the data collection  $\mathcal{D} = \{\mathcal{D}_1, \dots, \mathcal{D}_M\}$ . In particular, we wish to exploit that some structures or patterns are common among units.

Invariably, distinct units will differ in various ways, e.g., they may be of different design or construction, they may be in different condition, or they may operate under different conditions. The properties or conditions that make units distinct are referred to as the *context* of a unit. An observed context may be included in the dataset as an explanatory variable. An unobserved context must be treated as a latent variable to be inferred from data and it is only possible to make such inferences by studying data from multiple, related units. We assign the letter  $c$  to latent context variables.

We consider the underlying process  $p(x, y)$  that generates data for any unit in a population. Let  $c \in \mathbb{R}^K$  be a latent context variable with distribution  $p(c)$ . The context identifies a unit in the population supported by  $p(c)$ . We can then think of the process as the marginalization over all units, i.e.,  $p(x, y) = \int p(x, y|c)p(c)dc$ . With this model,  $p(x, y|c_i) = p_i(x, y)$ , for a given realization  $c = c_i$ . This implies that  $p(y|x, c_i) = p_i(y|x)$ , showing that we can model the behavior of all units by a single conditional distribution.

We now state that the goal of multi-unit soft sensing is to learn from  $\mathcal{D}$  a distribution  $q(y|x, c)$  that approximates  $p(y|x, c)$ . We contrast this to the single-unit soft sensing, where  $p_i(y|x)$  is approximated using  $\mathcal{D}_i$ , for  $i = 1, \dots, M$ ; that is, where  $M$  soft sensors are learned separately.

Our work aims to study empirically and theoretically the predictive performance of the approximation  $q(y|x, c)$ . First, we want to investigate how performance scales with the number of units  $M$ . Second, we want to examine the few-shot learning performance of  $q(y|x, c)$  as the context  $c$  is calibrated to few observations of a new unit (whose data was not used to learn  $q$ ).

### 3 Model description

We consider a hierarchical model of the observed target variables for a set of units. The model has three levels, as illustrated graphically in Figure 1. The top-level has *universal* parameters ( $\theta$ ) that are shared by all units and observations. The middle *unit layer* has parameters ( $c$  and  $\tau$ ) that capture the specificity of units. At the inner *observation level*, the target variable ( $y$ ) is explained by the explanatory variables ( $x$ ) and the context ( $c$ ) of the observed unit. The target observation is subject to a measurement error ( $\varepsilon$ ) with a unit-specific variance ( $1/\tau$ ). The relationship between these variables is modeled using the universal parameters ( $\theta$ ). The hierarchical structure allows the model to capture variations at the level of units and observations. A mathematical description of the model is given next.

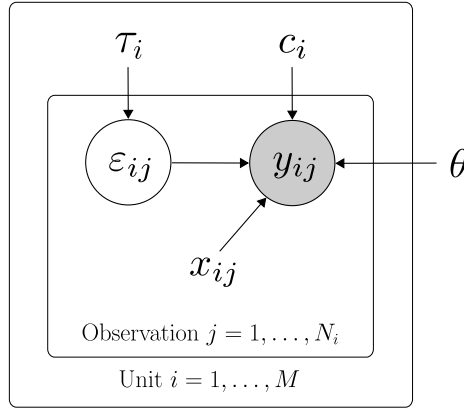


Figure 1: Multi-unit soft sensing model. Random variables are encircled. A grey (white) circle indicates that the variable is observed (latent). The nested plates (rectangles) group variables at different levels.

For unit  $i \in \{1, \dots, M\}$ , we model observation  $j \in \{1, \dots, N_i\}$  as

$$y_{ij} = f(x_{ij}; c_i, \theta) + \varepsilon_{ij}, \quad (1)$$

where  $\varepsilon_{ij}$  is the error term. The error, here interpreted as measurement noise, is modeled as  $\varepsilon_{ij} \sim \mathcal{N}(0, 1/\tau_i)$ , where the precision (or variance  $\sigma_i^2 = 1/\tau_i$ ) is allowed to differ between units. The function  $f$  is modeled by a neural network with parameters  $(c, \theta)$  and arguments  $x$ . A specific architecture of  $f$  is given later in the paper.

We can express the observation model as a conditional probability density:

$$y_{ij} | x_{ij}, c_i, \tau_i, \theta \sim p(y_{ij} | x_{ij}, c_i, \tau_i, \theta) = \mathcal{N}(y_{ij} | f(x_{ij}; c_i, \theta), 1/\tau_i). \quad (2)$$

The above model results from several simplifying assumptions: 1) the dimension of the context variables,  $K$ , is fixed and considered a design choice; 2) the model is conditional on  $x$ , and thus not a generative model of the observed data; 3) the model is homoscedastic since the measurement noise variance,  $\sigma_i^2$ , is fixed (per unit). Assumption 2 leads to a discriminative model which is suitable when the soft sensor will be used for on-line prediction. Relaxing assumption 3, for example by allowing  $\sigma_i$  to vary with  $x$ , would give a more complex heteroscedastic model, which may be harder to learn in a data-scarce setting.

### 3.1 Priors

The neural network parameters  $\theta$  are universal, i.e., shared by all units. We want the function  $f$  to behave smoothly, so that the effect of varying the unit-specific context parameters,  $c$ , leads to a predictable pattern. To regularize the neural network, we may impose on  $\theta$  a Gaussian prior,  $p(\theta) = \mathcal{N}(0, \Sigma_\theta)$ . This prior corresponds to an  $L^2$ -regularization of the  $\theta$ -parameters [25].

The context parameters,  $\mathbf{c}$ , are used to modulate  $f$  to fit the data of each unit. By putting a common prior on these parameters, we regularize the parameter-space. In this work, we use a common standard normal prior  $p(c_1) = \dots = p(c_M) = \mathcal{N}(0_K, I_K)$ . The identity covariance matrix is justified since the neural network  $f$  has the capacity to scale the context variables. Pinning the covariance matrix to the identity matrix simplifies modeling.

On the precision parameters,  $\tau_i$ , we put a gamma prior  $p(\tau_i) = \text{Gamma}(\alpha, \beta)$ , where the hyper-parameters  $\alpha$  and  $\beta$  are the concentration and rate, respectively. This prior corresponds to a zero-avoiding inverse-gamma prior on the variance [26]. For a normalized target variable  $y$ , we specify a weakly informative prior on the precision by setting  $\alpha = 1$  and  $\beta = 0.001$ . This setting gives a prior on the precision with expected value  $10^3$  and variance  $10^6$ .

The prior on  $(\mathbf{c}, \boldsymbol{\tau}, \theta)$  can be factorized as follows:

$$\log p(\mathbf{c}, \boldsymbol{\tau}, \theta) = \sum_{i=1}^M [\log p(c_i) + \log p(\tau_i)] + \log p(\theta). \quad (3)$$

### 3.2 Likelihood

We collect the variables in the following sets to allow a compact notation:  $\mathbf{x} = \{x_{ij}\}_{ij}$ ,  $\mathbf{y} = \{y_{ij}\}_{ij}$ ,  $\mathbf{c} = \{c_i\}_i$ , and  $\boldsymbol{\tau} = \{\tau_i\}_i$ . The log-likelihood can then be expressed as:

$$\ell(\mathbf{c}, \boldsymbol{\tau}, \theta | \mathcal{D}) := \log p(\mathbf{y} | \mathbf{x}, \mathbf{c}, \boldsymbol{\tau}, \theta) = \sum_{i=1}^M \sum_{j=1}^{N_i} \log p(y_{ij} | x_{ij}, c_i, \tau_i, \theta). \quad (4)$$

We use the short-form notation  $\ell(\mathbf{c}, \boldsymbol{\tau}, \theta | \mathcal{D})$  for the log-likelihood when it is considered as a function of the parameters  $(\mathbf{c}, \boldsymbol{\tau}, \theta)$ , given data  $\mathcal{D} = (\mathbf{x}, \mathbf{y})$ . In Section 4, we show how to perform MAP estimation of the parameters, given the log-likelihood in (4) and log-prior in (3).

## 4 Learning method

In model learning, the posterior density of the parameters  $(\mathbf{c}, \boldsymbol{\tau}, \theta)$  is of chief interest. The application of Bayes' theorem to the model in Section 3, yields:

$$p(\mathbf{c}, \boldsymbol{\tau}, \theta | \mathbf{x}, \mathbf{y}) \propto p(\mathbf{y} | \mathbf{x}, \mathbf{c}, \boldsymbol{\tau}, \theta) p(\mathbf{c}, \boldsymbol{\tau}, \theta), \quad (5)$$

where the posterior on the left-hand side is proportional to the joint density. The joint density is the product of the prior in (3) and likelihood in (4).

A maximum a posteriori (MAP) estimate of the parameters is sought by solving the following optimization problem:

$$(\hat{\mathbf{c}}, \hat{\boldsymbol{\tau}}, \hat{\theta}) = \arg \max_{\mathbf{c}, \boldsymbol{\tau}, \theta} p(\mathbf{c}, \boldsymbol{\tau}, \theta | \mathbf{x}, \mathbf{y}). \quad (6)$$

The point estimate,  $(\hat{\mathbf{c}}, \hat{\boldsymbol{\tau}}, \hat{\theta})$ , is of the mode of the parameters' posterior density. Next, we discuss how to solve this problem using a stochastic gradient ascent method. Our procedure follows standard practices in deep learning [25], with some adaptations to our multi-unit soft sensor model.

## 4.1 Optimization

In practice, MAP estimation is usually implemented as the maximization of an alternative objective function, here written as

$$J(\mathbf{c}, \boldsymbol{\tau}, \theta \mid \mathcal{D}) := \ell(\mathbf{c}, \boldsymbol{\tau}, \theta \mid \mathcal{D}) + \log p(\mathbf{c}, \boldsymbol{\tau}, \theta). \quad (7)$$

This objective function is obtained by taking the logarithm of the posterior in (5) and dropping the constant evidence term. These operations do not alter the solution (estimate), but make the objective simpler to optimize numerically. Note that all the terms making up  $J$  can be computed analytically for the densities specified in Section 3.

**Constrained precision estimation** The optimization problem above involves the implicit constraint that the target precision must be strictly positive, i.e.  $\tau_i > 0$ . To incorporate this constraint into an unconstrained gradient-based method, we reparameterize  $\tau_i$  as follows. Let  $\tau_i = g(t_i) = \log(1 + \exp(t_i))$ , where  $t_i \in \mathbb{R}$  is a new parameter. The reparameterization uses the softplus function  $g$ , which maps  $\mathbb{R} \rightarrow \mathbb{R}_{>0}$ . The softplus function is injective and does not change the solution.

We denote the reparameterized objective function by

$$J^r(\mathbf{c}, \mathbf{t}, \theta \mid \mathcal{D}) := \ell(\mathbf{c}, g(\mathbf{t}), \theta \mid \mathcal{D}) + \log p(\mathbf{c}, g(\mathbf{t}), \theta), \quad (8)$$

where  $\mathbf{t} = \{t_i\}_i$  and  $g(\mathbf{t})$  is the softplus function applied element-wise to  $\mathbf{t}$ .

**Stochastic gradients** Gradient-based optimization requires us to compute gradients of  $J^r$  in (8). Let  $\nabla J^r(\mathbf{c}, \mathbf{t}, \theta \mid \mathcal{D})$  denote the gradient of  $J^r$  with respect to the parameters  $(\mathbf{c}, \mathbf{t}, \theta)$  at some point in the parameter space (here unspecified). The gradient is conveniently computed using the back-propagation algorithm [27]. However, the computation becomes expensive for large datasets since the likelihood has  $|\mathcal{D}| = N = N_1 + \dots + N_M$  terms. To reduce the computational burden we resort to stochastic gradient estimates.

Let  $\mathcal{B} = (\mathcal{B}_1, \dots, \mathcal{B}_M)$  be a collection of randomly selected mini-batches  $\mathcal{B}_i \subset \mathcal{D}_i$  of size  $B_i = |\mathcal{B}_i|$ . The log-likelihood of task  $i$  can then be approximated as follows:

$$\sum_{x, y \in \mathcal{D}_i} \log p(y \mid x, c_i, \tau_i, \theta) \simeq \frac{N_i}{B_i} \sum_{x, y \in \mathcal{B}_i} \log p(y \mid x, c_i, \tau_i, \theta).$$

Using this, we can obtain a mini-batch approximation of  $J^r(\mathbf{c}, \mathbf{t}, \theta | \mathcal{D})$ :

$$\begin{aligned} J^r(\mathbf{c}, \mathbf{t}, \theta | \mathcal{B}) &= \sum_{i=1}^M \frac{N_i}{B_i} \sum_{(x,y) \in \mathcal{B}_i} \log p(y | x, c_i, g(t_i), \theta) \\ &\quad + \sum_{i=1}^M \log p(c_i) + \sum_{i=1}^M \log p(g(t_i)) + \log p(\theta). \end{aligned}$$

If  $\mathcal{B}_i = \emptyset$ , we set  $\log p(c_i) = \log p(g(t_i)) = 0$  in the above sum, effectively removing any contribution from unit  $i$  to the objective. A mini-batch stochastic gradient estimate  $\nabla J^r(\mathbf{c}, \mathbf{t}, \theta | \mathcal{B})$  can then be computed using back-propagation. Provided that the mini-batches are selected randomly (with substitution), the stochastic gradient is an unbiased estimate of  $\nabla J^r(\mathbf{c}, \mathbf{t}, \theta | \mathcal{D})$ . Pseudocode for the estimator is given in Algorithm 1.

---

**Algorithm 1** Stochastic gradient estimator

---

**Require:** data  $\mathcal{D}$ , model  $p(\mathbf{y}, \mathbf{c}, \boldsymbol{\tau}, \theta | \mathbf{x})$ , and parameter values  $(\mathbf{c}, \mathbf{t}, \theta)$ .

- 1: Randomly draw a mini-batch  $\mathcal{B}$  from  $\mathcal{D}$
- 2:  $\tilde{J} \leftarrow 0$
- 3: **for**  $i = 1, \dots, M$  **do**
- 4:     **if**  $\mathcal{B}_i \neq \emptyset$  **then**
- 5:         **for**  $(x, y) \in \mathcal{B}_i$  **do**
- 6:              $\tilde{J} \leftarrow \tilde{J} + (N_i/B_i) \log p(y | x, c_i, g(t_i), \theta)$
- 7:         **end for**
- 8:          $\tilde{J} \leftarrow \tilde{J} + \log p(c_i) + \log p(g(t_i))$
- 9:     **end if**
- 10: **end for**
- 11:  $\tilde{J} \leftarrow \tilde{J} + \log p(\theta)$
- 12: Compute  $\nabla \tilde{J}$  using back-propagation
- 13: **return**  $\nabla \tilde{J}$

---

**Mini-batch gradient ascent** We bring the above considerations together and present a mini-batch gradient ascent method for the MAP estimation problem in (6). First, we reformulate the problem to

$$(\hat{\mathbf{c}}, \hat{\mathbf{t}}, \hat{\theta}) = \arg \max_{\mathbf{c}, \mathbf{t}, \theta} J^r(\mathbf{c}, \mathbf{t}, \theta | \mathcal{D}), \quad (9)$$

where the reformulated objective is given by (8). Given an initial point for the parameters,  $(\mathbf{c}, \mathbf{t}, \theta)_0$ , we iteratively update the parameter values as

$$(\mathbf{c}, \mathbf{t}, \theta)_{k+1} = (\mathbf{c}, \mathbf{t}, \theta)_k + \lambda_k \nabla J^r(\mathbf{c}, \mathbf{t}, \theta | \mathcal{B})|_{(\mathbf{c}, \mathbf{t}, \theta) = (\mathbf{c}, \mathbf{t}, \theta)_k}, \quad (10)$$

where  $\lambda_k$  is the learning rate at step  $k$  and the gradient estimate is computed using Algorithm 1. Note that the mini-batch is randomly selected at each

iteration. The optimization is stopped when some termination criterion is met, and the final parameter values are returned as the estimate  $(\hat{\mathbf{c}}, \hat{\boldsymbol{\tau}}, \hat{\theta})$ , where the precision estimate is retrieved as  $\hat{\boldsymbol{\tau}} = g(\hat{\mathbf{t}})$ .

## 4.2 Context calibration

The previous sections describe how to learn a model from data  $\mathcal{D}$  collected from  $M$  units. Here, we provide a method for calibrating a learned model to data from new units; i.e., data that was not included in  $\mathcal{D}$  and that we get access to after having learned the initial model.

Let  $(\hat{\mathbf{c}}, \hat{\boldsymbol{\tau}}, \hat{\theta})$  be the parameters estimated from  $\mathcal{D}$ . We assign the index  $M+1$  to a new unit with data  $\mathcal{D}_{M+1}$ . A simple calibration procedure for  $c_{M+1}$  and  $\tau_{M+1}$  is to apply the gradient update in (10) with a fixed  $\theta = \hat{\theta}$  and  $\mathcal{B} = \mathcal{D}_{M+1}$ . With this procedure,  $K+1$  parameters are calibrated to  $|\mathcal{D}_{M+1}|$  data points. Provided that we do not have any prior knowledge about unit  $M+1$ , it is natural to initialize  $c_{M+1} = 0$  and  $\tau_{M+1} = (\hat{\tau}_1 + \dots + \hat{\tau}_M)/M$ .

The above calibration procedure works under the assumptions that  $|\mathcal{D}_{M+1}| \ll |\mathcal{D}|$  and that the  $\theta$  estimate has converged. When  $|\mathcal{D}_{M+1}|$  contains very few data points (relative to the task to be solved), the calibration procedure can be thought of as a few-shot learning method working on a pretrained model.

In the case where  $|\mathcal{D}_{M+1}|$  contains very few data points, it may also make sense to fix  $\tau_{M+1}$  during training to reduce the number of learned parameters.

## 4.3 Context parameter analysis

The context parameters in  $\mathbf{c}$  represent latent variables, and cannot be expected to exactly represent physical quantities. However, one may still hope that the learned context parameter space possess certain properties which are commonly held by physical parameter spaces. An important such property is that similar units are represented by similar context parameters. To investigate the validity of beliefs like this, methods for analysing the context parameters are required. In this section we describe an approach which may give an indication of whether the learned context parameter space is well-behaved; for example in the sense of being smooth.

**Laplace approximation** MAP estimation, as presented above, gives a point estimate  $(\hat{\mathbf{c}}, \hat{\boldsymbol{\tau}}, \hat{\theta})$  of the mode of the posterior distribution  $p(\mathbf{c}, \boldsymbol{\tau}, \theta | \mathcal{D})$ . Thus, it does not inform us of the uncertainty in the estimate. In the few-shot learning setting, the marginalized posterior distribution  $p(\mathbf{c} | \mathcal{D})$  may provide useful information about the context uncertainty given few observations, which may in turn be useful for analysing context parameters. While the exact posterior is hard to compute, a local approximation  $q(\mathbf{c} | \mathcal{D})$  of  $p(\mathbf{c} | \mathcal{D})$  can be obtained by Laplace's approximation [8]:

$$q(\mathbf{c} | \mathcal{D}) = \mathcal{N}(\mu_c = \hat{\mathbf{c}}, \Sigma_c = S_c) \quad (11)$$

$$S_c^{-1} = -\nabla_{\mathbf{c}} \nabla_{\mathbf{c}} J(\mathbf{c}, \hat{\boldsymbol{\tau}}, \hat{\theta} | \mathcal{D})|_{\mathbf{c}=\hat{\mathbf{c}}} \quad (12)$$

**Information gain estimation** The Kullback-Leibler divergence  $D_{\text{KL}}(p \parallel q)$  between two distributions can be interpreted as the *information gain* from  $p$  over  $q$ ; see [28]. The value of  $D_{\text{KL}}(p(\mathbf{c} \mid \mathcal{D}) \parallel p(\mathbf{c}))$  will then represent the total amount of information about the context parameter distribution given by the dataset  $\mathcal{D}$ , compared to the prior, in the unit of nat. Multiplying this number with  $\log_2(e)$ , we get the information gain in bits. Using Laplace’s approximation, described in (11), we can use the approximate posterior  $q(\mathbf{c} \mid \mathcal{D})$  to calculate an estimate  $D_{\text{KL}}(q(\mathbf{c} \mid \mathcal{D}) \parallel p(\mathbf{c}))$  of the informativity of a dataset  $\mathcal{D}$ .

This procedure may be applied to the sequential learning setting considered later, where sequences of datasets are constructed by adding one new data point at a time. If the parameter space is well-behaved in the manner described above, one should expect the information gain to vary smoothly with dataset size.

In general, smoothness of the information gain does not guarantee that similar units have similar context parameters after calibration (the problem of estimating  $c$  may be under-determined). However, it may indicate that the change in  $p(\mathbf{c} \mid \mathcal{D})$  as a function of  $\mathcal{D}$  is bounded. Thus, a smooth information gain suggests that units  $k$  and  $k + 1$  which are similar in the sense that they give rise to similar datasets  $\mathcal{D}_k$  and  $\mathcal{D}_{k+1}$  can at least be represented by context parameters  $c_k$  and  $c_{k+1}$  which are not too different.

## 5 Empirical study

We demonstrate the few-shot learning capabilities of our model by applying it as a *virtual flow meter* (VFM). This type of soft sensor is used in petroleum production to estimate multi-phase flow rates, which are typically challenging and expensive to measure directly [23]. Using an input  $x$  which consist of easily accessible measurements like pressure, temperature and valve opening, a VFM predicts a flow rate of interest  $y$ .

VFMs based on deep learning have shown promising results [20, 29]. However, it is commonly believed that their successful use requires large amounts of data [23]. Such a requirement would limit their applicability, since the wells with the best instrumentation (and hence, the most data) are typically also the wells were VFMs are needed the least. Thus, the application of VFM to wells with few observations provides an interesting case for few-shot learning.

In this section, we apply our proposed few-shot learning strategy to the soft sensing problem of virtual flow metering on a large industrial dataset. The result is a VFM strategy which, given a sufficiently large dataset gathered from other units, provides accurate predictions for new units, even when the number of observations can be counted on one hand.

In the following, a single petroleum well constitutes a unit. The soft sensor which results from applying this interpretation to our model is similar to the ones used in [20, 29] to perform multi-task learning across wells. However, the few-shot learning experiments conducted in this work considers a different data availability regime than the experiments presented in said works. Our model architecture also differs by its somewhat less problem-specific architecture as

well as its inclusion of a learnable precision parameter which is unique for each unit. Finally, we conduct our study on a larger number of wells than previous studies.

## 5.1 Dataset

The dataset consists of pairs  $(x_{ij}, y_{ij})$  of observations, where

$$\begin{aligned} x_{ij} &= [u_{ij}, p_{ij}^{\text{WH}}, p_{ij}^{\text{DC}}, T_{ij}^{\text{WH}}, \eta_{ij}^{\text{OIL}}, \eta_{ij}^{\text{GAS}}, Q_{ij}^{\text{GL}}], \\ y_{ij} &= Q_{ij}^{\text{TOT}}. \end{aligned}$$

Here,  $u$  denotes choke valve opening,  $p^{\text{WH}}$  and  $p^{\text{DC}}$  denote pressures at the wellhead and downstream the choke valve,  $T^{\text{WH}}$  denotes wellhead temperature,  $\eta^{\text{OIL}}$  and  $\eta^{\text{GAS}}$  denote volumetric oil and gas fractions,  $Q^{\text{GL}}$  denotes volumetric gas lift rate and  $Q^{\text{TOT}}$  denotes total volumetric flow rate. Each data point consists of an average value of each measurement taken over an interval where flow is close to steady-state, detected using the technology described in [30]. Before processing, the observations were shifted and scaled to approximately lie in the unit interval. The measurements of total flow rate includes both well tests and multi-phase flow meter measurements, which could be addressed by our model through the use of separate precision parameters for each instrument type, like done in [31]. However, for the sake of simplicity, we did not differentiate between the two types of data points in our experiments. The dataset consists of data from  $M = 80$  different wells. Splitting into training, validation and test sets was done differently in the two experiments which were conducted.

In the pretraining experiment, the data were split into training, validation and test sets using the method described in [20]. In total, the dataset consisted of 89 417 data points of which 81%, 14% and 5% were assigned to the training, validation and test sets, respectively. A more detailed illustration of the dataset partition is shown in Figure 2. As can be seen from the figure, the wells present in the dataset cover a large range of settings with regards to data frequency and time span.

## 5.2 Pretraining

The model parameters  $(\mathbf{c}, \boldsymbol{\tau}, \theta)$  can be estimated from data by using the gradient ascent method of (10) along with Algorithm 1. Since the dimension of  $\theta$  exceeds the dimensions of  $\mathbf{c}$  and  $\boldsymbol{\tau}$  by orders of magnitude for our model, one can expect that most of the complexity of this learning problem can be attributed to the estimation of gradients with respect to  $\theta$ . Thus, it would be convenient to identify conditions which justify not updating  $\theta$ , instead only estimating  $(\mathbf{c}, \boldsymbol{\tau})$ .

To guide the search for such conditions, one can consider the theoretical convergence rate of the MAP estimator. Assuming that the units are sufficiently similar, and that each unit contributes with a comparable number of data points which does not change with  $M$ , the theoretical expected learning rate as a function of the number  $M$  of units in the dataset will, in a large number of

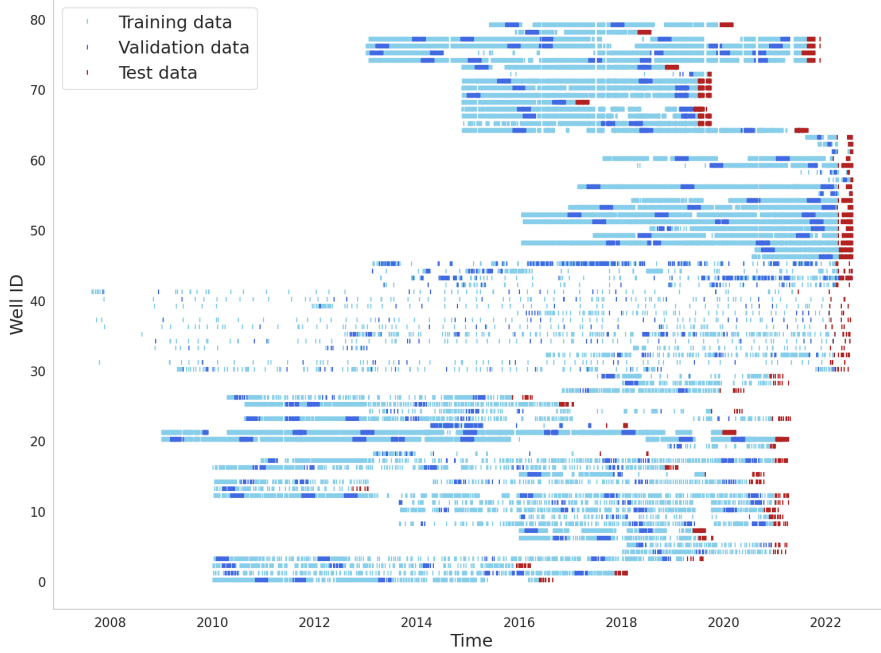


Figure 2: Partition of available data points into training (light blue), validation (dark blue) and test (red) sets. A rectangular marker indicates the availability of a single data point. Rectangles may overlap.

multi-task learning settings, be  $\mathcal{O}(1/\sqrt{M})$  [12]. Since this function flattens out as  $M$  increases, one should expect diminishing returns from each single new well as their number increases.

We tested this assumption by training and estimating the performance of a model on data for  $M = 1, 5, 10, 20, 40, 80$  units. For each value of  $M$ , the dataset was randomly divided into  $\frac{80}{M}$  disjoint groups of  $M$  different units. Then, a model was learned from the data from each group using the method described in Section 4. Implementation details are described in Appendix A.

After training, the model was evaluated on a previously unseen test set drawn from the same wells as its training set (as illustrated by Figure 2). This procedure was repeated 20 times with different random seeds to reduce noise due to well group partitioning, and from stochasticity related to neural network training.

Figure 3 shows the test set MSE, averaged over all wells and experiment repetitions, as a function of the number of units from which data were available during training. In addition, the figure shows a function in  $\mathcal{O}(1/\sqrt{M})$  fitted to this curve using least squares regression. From the figure, one can see that the theoretically motivated convergence rate lies close to the observed one. Further-

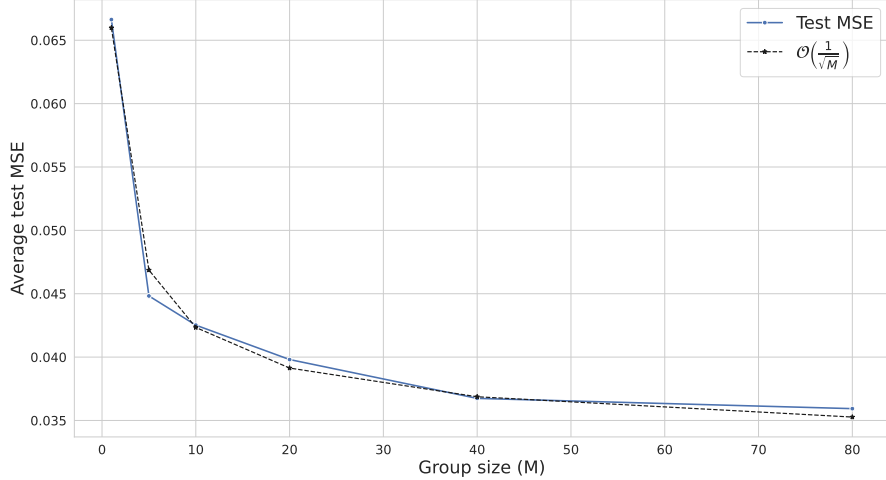


Figure 3: MTL performance for increasing number of wells.

more, one can see that the prediction error flattens out significantly between 40 and 80 wells.

Averages over wells for each individual experiment run is shown in Figure 7 in Appendix C.

### 5.3 Few-shot learning performance

The intention of the few-shot learning experiment was to simulate a data-scarce setting where new measurements appear at regular but infrequent intervals. Since this is not the case for the dataset used in the preceding section, the few-shot learning experiment required data to be drawn using a different strategy from the one illustrated by Figure 2. The strategy which was used simulates a data-scarce setting in which data points appear one at a time with low frequency, and is described in Appendix B.

In the following, the wells were partitioned into two sets: The set of *base wells*, which provide many data points and are used for model pre-training, and the set of *holdout wells*, which provide few data points and are used to evaluate few-shot learning performance.

In the first step of the experiment, the procedure described in Section 4 was used to learn a base model from a base training set consisting of all available data from 60 randomly chosen base wells. The reason for choosing this particular number of base wells was largely motivated by the need for a holdout set of a size sufficient for robust evaluation of model performance. However, we argue that  $M = 60$  is situated safely in what can be considered a flat part of Figure 3, justifying freezing the value  $\theta$  learned from the 60 base wells.

Pretraining resulted in a base model with parameters  $(\hat{\theta}, \hat{c}, \hat{\tau})$ . This model

was used in the succeeding calibration step, which was performed for each of the 20 holdout wells  $k > M$ . Here, the neural network parameters  $\theta = \hat{\theta}$  were fixed at their value from pretraining, the precision parameter was kept fixed at  $\hat{\tau}_k = (\hat{\tau}_1 + \dots + \hat{\tau}_M)/M$ , while the context parameter  $c_k$  was calibrated to datasets of increasing size from the holdout well (from 0 all the way up to 10 data points), using the method described in Section 4.2. Further implementation details are given in Appendix A.

To increase the statistical strength of the experiment, this procedure was repeated 20 times with different random choices of the 60 base wells. This resulted in each of the 80 wells appearing in the set of holdout wells at least once. To enable cross-unit comparison, a randomly chosen experiment run was chosen to represent the few-shot learning performance of the calibrated model on each well.

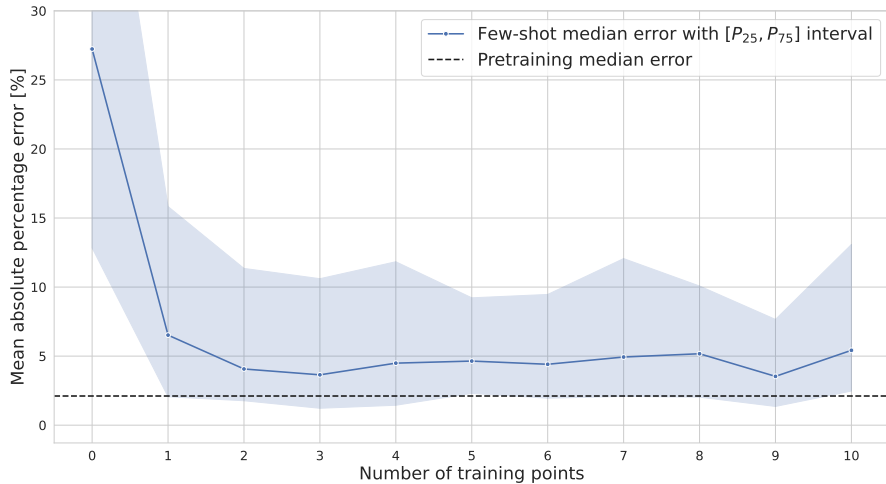


Figure 4: Few-shot learning performance. The pretrained models had access to an average of 903 data points from each well.

Figure 4 describes the development of the mean absolute percentage error (MAPE) on the test set as the number of available data points increases. Here, the blue line shows the median test MAPE across wells, and the colored region shows 50% probability intervals over all wells. The black dashed line indicates the 2.11% MAPE achieved by the base model when evaluated in the same way as the few-shot learning model on the first week of the test set shown in Figure 2.

#### 5.4 Analysis of context posteriors

Figure 5 describes the information gain  $D_{\text{KL}}(q(\mathbf{c} | \mathcal{D}_k) \| p(\mathbf{c}))$  for holdout datasets  $\mathcal{D}_k$  of increasing size, as estimated by the procedure described in Section 4.3.

The blue line shows the information gain as a function of dataset size, while the shaded blue region shows 50% probability intervals calculated across wells. One can see from the figure that dataset information gain increases steadily with dataset size. Furthermore, the slope of the curve seems to be decreasing, indicating that the effect of additional data points are diminishing.

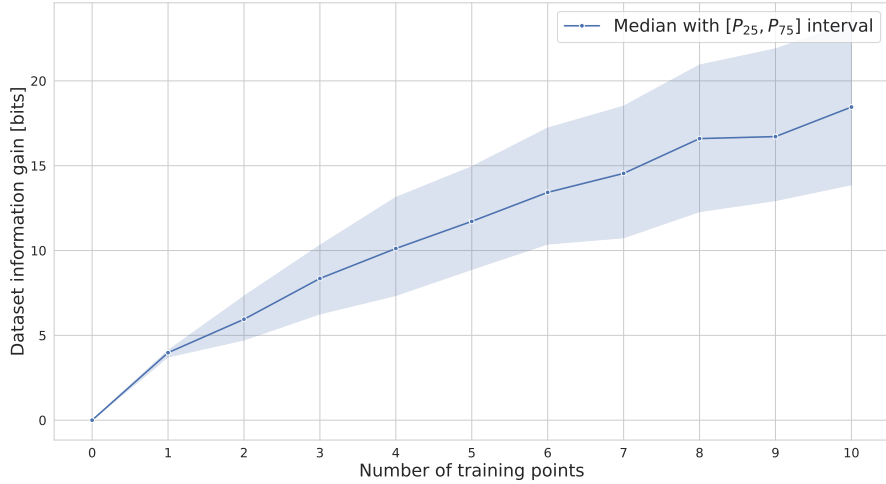


Figure 5: Information gain of datasets with increasing size.

## 6 Concluding remarks

Figure 3 suggests that the convergence rate of  $\mathcal{O}(1/\sqrt{M})$ , where  $M$  is the number of units, applies well to the soft sensing problem of virtual flow metering. The flatness of this convergence rate for large values of  $M$  serves as motivation for our proposed few-shot learning approach, where a pretrained model with fixed parameters acts as a base model. The result is a data efficient learning algorithm, where only the low-dimensional context parameters are calibrated to data from a new unit.

As shown by the results in Figure 4, our proposed calibration procedure only requires a handful of training data points for the resulting model to perform well on a previously unseen unit. We highlight that the median error across new units drops below 5% after calibration to only three data points, which can be considered as a high performance for a virtual flow meter [31].

While being data efficient on new tasks, we have to remark that the performance is enabled by a base model, which is learned from a large number of data points gathered from a varied set of units. In a sense then, our method is not operating in a low-data regime. We still argue that our method should be classified as highly data-efficient, since it yields high performance on units with

very few data points. In this setting, one should not expect high performance from a single-unit data-driven soft sensor. Using our proposed approach, a base model can be trained on data from multiple units, and then applied as a soft sensor in settings where deep learning-based approaches were earlier believed to be inappropriate.

From Figure 5, one can see that the median dataset information gain varies smoothly with dataset size. This indicates that the regularization which is introduced by the prior distribution over the context variable reduces the complexity of the learned context parameter space. The smoothness of the parameter space as well as its low dimension suggests that the learned context parameters may be meaningful to the model, even if they do not permit a physical interpretation.

In conclusion, we have demonstrated empirically that our multi-unit soft sensing model can represent a large range of process realizations or units, and that it can provide accurate predictions for new units after calibration to only a handful of observations – not unlike a mechanistic model.

## Acknowledgements

This work was supported by Solution Seeker AS.

## A Implementation details

This section describes in further detail how the model in Section 3 and learning algorithm in Section 4 were implemented in the case study of Section 5.

### A.1 Model

The multi-unit soft sensor was modeled using a deep neural network, implemented in PyTorch [32]. The network architecture, shown in Figure 6, is similar to the architecture used for meta-learning in [22]. It consists of a feed-forward neural network of width 400 and depth 4, with ReLU activation functions. Its input is the concatenation of the input data point  $x_{ij}$  and a learnable context vector  $c_i$  of dimension 10, which is unique for each unit. Given  $x_{ij}$ , the neural network returns an estimate  $\hat{y}_{ij} = f(x_{ij}; c_i, \theta)$  of the mean of  $y_{ij}$ . Together with a precision parameter acquired by passing the learnable unit-specific parameter  $t_i$  through the softmax function  $g$ , this estimate is used to form the conditional distribution

$$p(y_{ij} | x_{ij}, c_i, t_i, \theta_i) = \mathcal{N}(y_{ij} | f(x_{ij}; c_i, \theta), 1/g(t_i)).$$

### A.2 Learning method

**Pretraining** During pretraining, all model parameters  $(\mathbf{c}, \mathbf{t}, \theta)$  were learned jointly through the mini-batch gradient ascent procedure described in Section

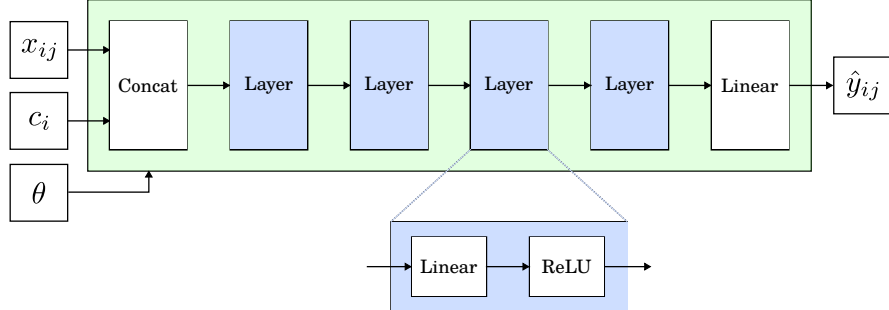


Figure 6: Neural network architecture implementing  $f(x; c, \theta)$ . A data point  $x_{ij}$  from unit  $i$  is processed to produce a prediction  $\hat{y}_{ij}$ .  $\theta$  is the parameters of the linear layers in the network and  $c_i$  is the context parameters of unit  $i$  (whose data is being processed). The precision parameter  $\tau_i$  is not shown.

4.1, using the Adam optimizer [33] with a batch size of 2048. For both the convergence rate experiment described in Section 5.2 and the few-shot learning experiment described in Section 5.3, training was run for 20 000 epochs with a learning rate of  $1 \cdot 10^{-4}$ . In both cases, the model with the lowest validation set MSE was returned. The training was conducted on a desktop computer with a single GPU.

**Calibration** Calibration of context parameters  $c_k$  to previously unseen units  $k > M$  was done using the procedure described in Section 4.2. For each new data point, the context parameter  $c_k$  was reinitialized and training was done from scratch. This training consisted of 100 epochs of stochastic gradient ascent with a learning rate of  $1 \cdot 10^{-4}$ . Due to the low data availability, no model selection procedures were performed in this setting.

## B Model validation in few-shot learning

The dataset described in Section 5.1 consists of data from wells with significant differences in instrumentation and practice of operation. As can be seen in Figure 2, this results in significant differences between wells in data frequency as well as dataset duration. To increase the comparability of results across wells, we devised a procedure inspired by the way in which new well tests typically arrive in a petroleum production setting. The result was the following procedure, which was used for each of the unseen wells  $k > M$ :

1. Set  $\mathcal{D}_k = \emptyset$
2. For  $j = 1, \dots, 10$  :

- (a) Set  $(x_{kj}, y_{kj})$  to be the next available data point which is situated a week or more into the future, and add  $(x_{kj}, y_{kj})$  to the dataset  $\mathcal{D}_k$
- (b) Calibrate  $c_k$  to the dataset  $\mathcal{D}_k$
- (c) Evaluate the prediction error of the model on all available data from the week following the latest data point in  $\mathcal{D}_k$ . If no data is available, use the single next available data point as test set.

In this procedure, the division into training, validation and test sets shown in Figure 2 was ignored, and all data from each given well was used when running the procedure described above.

The relation between available measurements and the outflow of an oil well is known to change significantly over time [29], which is why the test set is limited to have a duration of one week. This results in the test set size differing between wells. However, the error metrics used take the form of averages, which means that test set size does not affect the magnitude of the error metric for a given well. Thus, we argue that the aggregation of results done later can be justified, even though the statistical strength of the test set error may differ between wells due to differing test set sizes.

## C Additional results

Figure 7 shows each of the 20 individual pretraining experiments. The variance observed between individual experiments supports the large number of experiment repetitions performed when generating Figure 3.

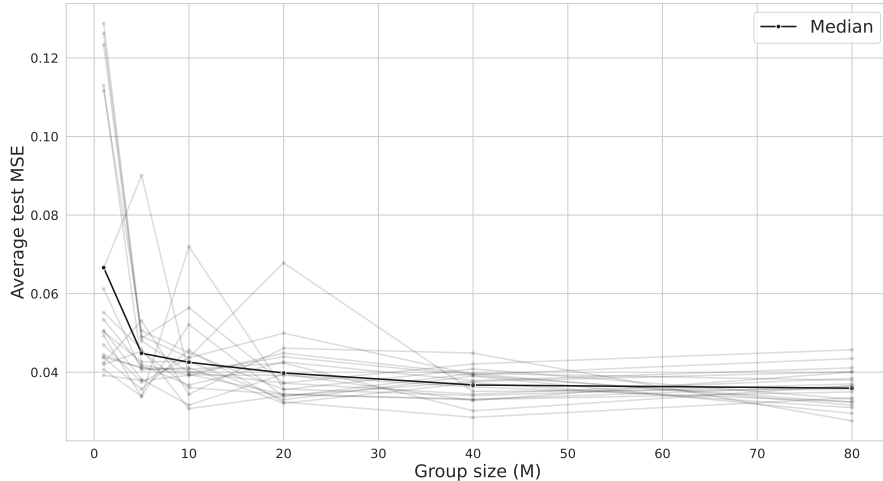


Figure 7: MTL performance for increasing number of  $M$ . Median across runs is shown in black, individual runs are shown in gray.

## References

- [1] Luigi Fortuna et al. *Soft sensors for monitoring and control of industrial processes*. en. 1st ed. Advances in industrial control. London: Springer, 2007. ISBN: 978-1-84628-479-3. DOI: <https://doi.org/10.1007/978-1-84628-480-9>.
- [2] Petr Kadlec, Bogdan Gabrys, and Sibylle Strandt. “Data-driven Soft Sensors in the process industry”. In: *Computers and Chemical Engineering* 33.4 (2009), pp. 795–814. ISSN: 00981354. DOI: 10.1016/j.compchemeng.2008.12.012.
- [3] Yuchen Jiang et al. “A Review on Soft Sensors for Monitoring, Control, and Optimization of Industrial Processes”. In: *IEEE Sensors Journal* 21.11 (2021), pp. 12868–12881. ISSN: 1530-437X. DOI: 10.1109/JSEN.2020.3033153.
- [4] Xiaofeng Yuan et al. “A Deep Supervised Learning Framework for Data-Driven Soft Sensor Modeling of Industrial Processes”. In: *IEEE Transactions on Neural Networks and Learning Systems* 31.11 (2020), pp. 4737–4746. ISSN: 21622388. DOI: 10.1109/TNNLS.2019.2957366.
- [5] Qingqiang Sun and Zhiqiang Ge. “A Survey on Deep Learning for Data-Driven Soft Sensors”. In: *IEEE Transactions on Industrial Informatics* 17.9 (2021), pp. 5853–5866. ISSN: 1551-3203. DOI: 10.1109/TII.2021.3053128. URL: <https://ieeexplore.ieee.org/document/9329169/>.
- [6] Zhiqiang Ge et al. “Data Mining and Analytics in the Process Industry: The Role of Machine Learning”. en. In: *IEEE Access* 5 (2017), pp. 20590–20616. ISSN: 2169-3536. DOI: 10.1109/ACCESS.2017.2756872. (Visited on 09/06/2023).
- [7] Erik Esche et al. “Semi-supervised learning for data-driven soft-sensing of biological and chemical processes”. In: *Chemical Engineering Science* 251 (2022), p. 117459. ISSN: 00092509. DOI: 10.1016/j.ces.2022.117459. eprint: 2107.13822.
- [8] Christopher M. Bishop. *Pattern recognition and machine learning*. 2006. ISBN: 978-0-387-31073-2.
- [9] Francesco Curreri, Luca Patanè, and Maria Gabriella Xibilia. “Soft sensor transferability: A survey”. In: *Applied Sciences* 11.16 (2021), pp. 1–18. ISSN: 20763417. DOI: 10.3390/app11167710.
- [10] Naiju Zhai et al. “Soft Sensor Model for Billet Temperature in Multiple Heating Furnaces Based on Transfer Learning”. en. In: *IEEE Transactions on Instrumentation and Measurement* 72 (2023), pp. 1–13. ISSN: 0018-9456, 1557-9662. DOI: 10.1109/TIM.2023.3267520. (Visited on 08/18/2023).

[11] Sinno Jialin Pan and Qiang Yang. “A Survey on Transfer Learning”. en. In: *IEEE Transactions on Knowledge and Data Engineering* 22.10 (Oct. 2010), pp. 1345–1359. ISSN: 1041-4347. DOI: 10.1109/TKDE.2009.191. (Visited on 09/13/2023).

[12] Yu Zhang and Qiang Yang. “A Survey on Multi-Task Learning”. In: *IEEE Transactions on Knowledge and Data Engineering* 4347.c (2021), pp. 1–20. DOI: 10.1109/TKDE.2021.3070203.

[13] Yuxin Huang et al. “Modeling Task Relationships in Multivariate Soft Sensor With Balanced Mixture-of-Experts”. en. In: *IEEE Transactions on Industrial Informatics* 19.5 (May 2023), pp. 6556–6564. ISSN: 1551-3203, 1941-0050. DOI: 10.1109/TII.2022.3202909. (Visited on 08/18/2023).

[14] Yu Da Hsiao, Jia Lin Kang, and David Shan Hill Wong. “Development of robust and physically interpretable soft sensor for industrial distillation column using transfer learning with small datasets”. In: *Processes* 9.4 (2021). ISSN: 22279717. DOI: 10.3390/pr9040667.

[15] Zheng Chai et al. “A Deep Probabilistic Transfer Learning Framework for Soft Sensor Modeling With Missing Data”. en. In: *IEEE Transactions on Neural Networks and Learning Systems* 33.12 (Dec. 2022), pp. 7598–7609. ISSN: 2162-237X, 2162-2388. DOI: 10.1109/TNNLS.2021.3085869. URL: <https://ieeexplore.ieee.org/document/9454563/> (visited on 08/15/2023).

[16] Xiangrui Zhang et al. “Deep Subdomain Learning Adaptation Network: A Sensor Fault-Tolerant Soft Sensor for Industrial Processes”. In: *IEEE Transactions on Neural Networks and Learning Systems* (2023), pp. 1–12. ISSN: 2162-237X, 2162-2388. DOI: 10.1109/TNNLS.2022.3231849.

[17] Yi Liu et al. “Domain adaptation transfer learning soft sensor for product quality prediction”. In: *Chemometrics and Intelligent Laboratory Systems* 192.April (2019), p. 103813. ISSN: 18733239. DOI: 10.1016/j.chemolab.2019.103813.

[18] Shifu Yan and Xuefeng Yan. “Joint monitoring of multiple quality-related indicators in nonlinear processes based on multi-task learning”. en. In: *Measurement* 165 (Dec. 2020), p. 108158. ISSN: 02632241. DOI: 10.1016/j.measurement.2020.108158. (Visited on 08/18/2023).

[19] Junfei Qiao, Jianglong Zhou, and Xi Meng. “A Multitask Learning Model for the Prediction of NOx Emissions in Municipal Solid Waste Incineration Processes”. en. In: *IEEE Transactions on Instrumentation and Measurement* 72 (2023), pp. 1–14. ISSN: 0018-9456, 1557-9662. DOI: 10.1109/TIM.2022.3225056.

[20] Anders T. Sandnes, Bjarne Grimstad, and Odd Kolbjørnsen. “Multi-task learning for virtual flow metering”. In: *Knowledge-Based Systems* 232 (2021), p. 107458. ISSN: 09507051. DOI: 10.1016/j.knosys.2021.107458. eprint: 2103.08713.

- [21] Chelsea Finn, Pieter Abbeel, and Sergey Levine. “Model-agnostic meta-learning for fast adaptation of deep networks”. In: *34th International Conference on Machine Learning, ICML 2017* 3 (2017), pp. 1856–1868.
- [22] Luisa Zintgraf et al. “Fast context adaptation via meta-learning”. In: *36th International Conference on Machine Learning, ICML 2019* 2019-June.2018 (2019). arXiv: 1810.03642 ISBN: 9781510886988, pp. 13262–13276.
- [23] Timur Bikmukhametov and Johannes Jäschke. “First Principles and Machine Learning Virtual Flow Metering: A Literature Review”. In: *Journal of Petroleum Science and Engineering* 184 (Jan. 2020). ISSN: 09204105. DOI: 10.1016/j.petrol.2019.106487.
- [24] Weisong Shi et al. “Edge Computing: Vision and Challenges”. en. In: *IEEE Internet of Things Journal* 3.5 (Oct. 2016), pp. 637–646. ISSN: 2327-4662. DOI: 10.1109/JIOT.2016.2579198. (Visited on 09/08/2023).
- [25] Ian Goodfellow, Yoshua Bengio, and Aaron Courville. *Deep Learning*. MIT Press, 2016. ISBN: 978-0-262-03561-3.
- [26] Andrew Gelman et al. *Bayesian Data Analysis*. 3rd. CRC Press, 2014. ISBN: 978-1-4398-9820-8.
- [27] David E Rumelhart, Geoffrey E Hinton, and Ronald J Williams. “Learning representations by back-propagating errors”. en. In: *Nature* 323 (1986), pp. 533–536. DOI: 10.1038/323533a0.
- [28] Solomon Kullback and Richard A Leibler. “On information and sufficiency”. In: *The annals of mathematical statistics* 22.1 (1951), pp. 79–86.
- [29] Mathilde Hotvedt, Bjarne A Grimstad, and Lars S. Imsland. “Passive learning to address nonstationarity in virtual flow metering applications”. In: *Expert Systems With Applications* 210.February (2022), p. 118382. ISSN: 0957-4174. DOI: 10.1016/j.eswa.2022.118382. URL: <https://doi.org/10.1016/j.eswa.2022.118382>.
- [30] B Grimstad et al. “A simple data-driven approach to production estimation and optimization”. In: *SPE intelligent energy international conference and exhibition*. OnePetro. 2016.
- [31] Bjarne Grimstad et al. “Bayesian neural networks for virtual flow metering: An empirical study”. en. In: *Applied Soft Computing* 112 (Nov. 2021), p. 107776. ISSN: 15684946. DOI: 10.1016/j.asoc.2021.107776. (Visited on 01/03/2023).
- [32] Adam Paszke et al. “PyTorch: An Imperative Style, High-Performance Deep Learning Library”. In: *Advances in Neural Information Processing Systems* 32 (2019), pp. 8026–8037.
- [33] Diederik P. Kingma and Jimmy Lei Ba. “Adam: A method for stochastic optimization”. In: *3rd International Conference on Learning Representations*. 2015, pp. 1–15.